

# Motion of active tracer in a lattice gas with cross-shaped particles

Cite as: J. Chem. Phys. 150, 144508 (2019); doi: 10.1063/1.5085769

Submitted: 14 December 2018 • Accepted: 19 March 2019 •

Published Online: 11 April 2019



Rakesh Chatterjee,<sup>1</sup>  Nimrod Segall,<sup>1</sup>  Carl Merrigan,<sup>2</sup>  Kabir Ramola,<sup>2,3</sup>  Bulbul Chakraborty,<sup>2</sup>  and Yair Shokef<sup>1</sup> 

## AFFILIATIONS

<sup>1</sup>School of Mechanical Engineering and Sackler Center for Computational Molecular and Materials Science, Tel Aviv University, Tel Aviv 69978, Israel

<sup>2</sup>Martin Fisher School of Physics, Brandeis University, Waltham, Massachusetts 02454, USA

<sup>3</sup>Centre for Interdisciplinary Sciences, Tata Institute of Fundamental Research, Hyderabad 500107, India

**Note:** This article is part of the Special Topic “Chemical Physics of Active Matter” in J. Chem. Phys.

## ABSTRACT

We analyze the dynamics of an active tracer particle embedded in a thermal lattice gas. All particles are subject to exclusion up to third nearest neighbors on the square lattice, which leads to slow dynamics at high densities. For the case with no rotational diffusion of the tracer, we derive an analytical expression for the resulting drift velocity  $v$  of the tracer in terms of non-equilibrium density correlations involving the tracer particle and its neighbors, which we verify using numerical simulations. We show that the properties of the passive system alone do not adequately describe even this simple system of a single non-rotating active tracer. For large activity and low density, we develop an approximation for  $v$ . For the case where the tracer undergoes rotational diffusion independent of its neighbors, we relate its diffusion coefficient to the thermal diffusion coefficient and  $v$ . Finally, we study dynamics where the rotation of the tracer is limited by the presence of neighboring particles. We find that the effect of this rotational locking may be quantitatively described in terms of a reduction in the rotation rate.

Published under license by AIP Publishing. <https://doi.org/10.1063/1.5085769>

## I. INTRODUCTION

A rich variety of dynamics can occur in assemblies of particles which display independent persistent motion. Such collections, referred to as “active materials,” are realized in several natural contexts such as proteins or motors inside cells,<sup>1,2</sup> monolayers of migrating cells,<sup>3,4</sup> bacterial suspensions,<sup>5</sup> pedestrians at crowded events,<sup>6</sup> and even traffic jams. At moderate densities, active particles with simple repulsive interactions can separate into inhomogeneous regions of liquid and gas, a phenomenon termed Motility-Induced Phase Separation or MIPS.<sup>7–9,46</sup> When confined to even higher densities, active materials can crystallize,<sup>10</sup> become jammed,<sup>11</sup> undergo glass transitions,<sup>12–14</sup> or even exhibit gelation.<sup>15,16</sup> However, since active particles strongly perturb (and are perturbed by) the motion of the particles around them, predicting the collective dynamics of such systems is difficult. In this paper, we address the simpler problem of a single active particle in a dense environment, in particular,

a system that exhibits glassy dynamics in the absence of activity due to inherent geometric frustration.

Many physical phenomena may be described by simplified theoretical models. Specifically, discrete lattice models have been shown to be useful in understanding equilibrium phase transitions, as well as non-equilibrium phenomena ranging from the glass transition<sup>17,18</sup> to the dynamics of active matter.<sup>19</sup> Lattice-gas models with different sizes of the excluded-volume region around each particle have a long history of study.<sup>18,20–31</sup> As solid-liquid phase transitions in real fluids are mediated by strong short-ranged repulsive forces, hard-core exclusion models are useful first approximations, and indeed, exhibit many of the same features found in simple fluids, structural glasses, and granular materials.

In this paper, we study a lattice gas of hard cross-shaped particles on the square lattice. In this model, which is also termed the  $N3$  model, each cross prevents the occupation of its first, second, and third nearest neighbors;<sup>20,22</sup> see Fig 1. It is the simplest lattice gas

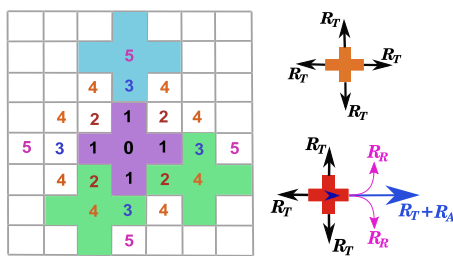


**FIG. 1.** Sites neighboring the center of a cross-shaped particle (purple) are numbered by their proximity to the center of the particle (site 0). Positions up to the third nearest neighbors are excluded for centers of neighboring particles. Another particle can only sit at a fourth (green), fifth (blue), or higher-order nearest-neighbor positions. With rotational locking, fourth-order neighbors prevent rotation. Dynamics are shown for a passive particle (orange) with only the thermal rate  $R_T$ , and for the active tracer (red) with the thermal rate  $R_T$ , active rate  $R_A$ , and rotation rate  $R_R$ ; small blue arrowhead at the center of the active tracer denotes its active direction.

model which displays a first-order phase transition to a crystal with increasing density, occurring at a melting density of  $\rho_m \approx 0.16$ .<sup>26</sup> Several studies have focused on the glassy behavior which results when the density of the system is quenched past this transition through random packing.<sup>18,28</sup> The supercooled branch is predicted to terminate at  $\rho_g \approx 0.17$ . The reason for this is that this model has competing close-packed configurations with opposite chirality and is thus geometrically frustrated. Conflicts between these incompatible ordered structures in the same region lead to a strong suppression of the dynamics.<sup>24</sup>

Here we introduce to this passive  $N3$  model a single active tracer particle, which in addition to taking thermal steps in each of the four lattice directions also takes active steps along the direction in which it is oriented. Additionally, the tracer also performs rotational diffusion. Although thermal tracer motion has been very well studied experimentally and theoretically, much less is known about active or driven tracers. Recent studies have focused on externally driven tracers,<sup>32–34</sup> active tracer motion,<sup>35–37</sup> as well as actively moving particles near the jamming transition.<sup>11</sup> Tracer motion in an embedding fluid is also an important theoretical problem in non-equilibrium statistical physics.<sup>38,39</sup>

We introduce activity to the  $N3$  model because that model exhibits glassy dynamics with increasing density. We, therefore, expect our results to aid in the understanding of the interplay between activity and slow dynamics in frustrated systems. Finally, cross-shaped particles are also interesting since, owing to their shape, it is possible for a particle to limit the rotation of its neighbors (locking). In this paper, we study the system with and without such rotational locking and find that it has a significant effect on the tracer's dynamics. Rotational locking should have important consequences for collective effects in all-active systems, which we will study in a subsequent publication.

The paper is organized as follows. In Sec. II, we introduce the model and describe the simulation details. In Sec. III, we study the case of an active tracer particle that does not change orientation. We derive an analytical expression for its resulting steady-state drift velocity in terms of nonequilibrium density correlations involving the tracer and the passive particles in its vicinity. Surprisingly, we find that the properties of the passive system are not enough to

fully describe the single active tracer, even in the low-activity and low-density limit. However, we do develop a theory in terms of equilibrium correlators, which is applicable in the low-density yet strong-activity regime. In Sec. IV, we study the motion of the tracer with free rotational diffusion, i.e., the active direction stochastically changes orientation independent of its neighbors. We obtain a theoretical result for the self-diffusion of the rotating active tracer in terms of the self-diffusion of a passive tracer and the drift velocity of a non-rotating tracer. Finally, in Sec. V, we turn our attention to the physically relevant but much less-studied case, where particle shape affects the rotational diffusion of the tracer (rotational locking). We show that many of the results from Sec. IV are still applicable with a reduced effective “rotation rate” compared to the rotation attempt rate. Since few studies have analyzed active or driven systems with rotational locking, our present study of a single active tracer lays the ground-work for the investigation of systems with a finite density of such active particles.

## II. MODEL

We study the lattice gas of particles with exclusion up to the third nearest neighbor on the square lattice. Figure 1 shows the equivalence of this exclusion to hard-core cross-shaped particles. Particles attempt to move to each one of their four nearest-neighbor sites at a fixed “thermal rate”  $R_T$ . We introduce a single active tracer particle into the system which is characterized by a self-propulsion direction (north, south, east, or west), along which it attempts to move with an “active rate”  $R_A$ . This active motion of the tracer is in addition to the thermal moves in all four directions. The active particle attempts to rotate its active direction by  $\pm \frac{\pi}{2}$ , to either direction at a rotation rate  $R_R$ ; see Fig. 1. In active systems, the ratio of active propulsion and thermal motion is usually referred to as the Péclet number; thus, here we identify it as  $Pe = \frac{R_A}{R_T}$ . In the absence of rotational locking, the rotational diffusion is given by the rotation rate  $R_R$ . The dynamics of our model are equivalent to those used for the simple exclusion active lattice gas studied in Ref. 40. However, as we show below, the slightly extended range of the interactions gives rise to new and interesting phenomena.

Moves to a new site are accepted if they do not create overlaps between any two crosses, i.e., exclusion up to third nearest neighbor. For rotation events, we consider two different versions of the dynamics. In the first version, rotations are always allowed whenever they are attempted, while in the second version, crosses in fourth-order neighboring sites prevent one another from changing the direction. The rotational-locking case may be interpreted in the following way: active particles that have a rigid structure must physically rotate in order for the particle to change the direction. Rotational locking may also be thought of as a useful approximation for active particle which are able to exert torques. We find that analysis of the freely rotating case is helpful in understanding systems with rotational locking, where the particles can be described as rotating with a modified rate.

Throughout this paper, we limit ourselves to the range of densities  $\rho < \rho_m \approx 0.16$  that is below the first-order phase transition; hence, the bath of passive particles always reaches equilibrium and does not get arrested in glassy states and, moreover, is in a homogeneous state before the phase separation that occurs at higher densities. We run dynamical Monte Carlo simulations on a periodic lattice of

dimension  $L \times L$ . We typically use  $L = 100$ , while for very low densities below  $\rho = 0.01$  to get reasonable statistics with enough particles in the lattice, we increased the system size to  $L = 500$ . We also increased system size to verify convergence in situations with high drift velocity, where the particle could cross the entire periodic lattice without the environment being randomized by thermal moves. We measure time in units of  $R_T$ . We first allow the system to relax for time  $t = 10^5$ , and then we start measuring the drift velocity or diffusion coefficient, until  $t = 10^6$ .

### III. NON-ROTATING ACTIVE TRACER

Here we consider the zero-rotation-rate limit  $R_R = 0$ . This is interesting in its own right, but as we will show in Secs. IV and V, this limit serves as the basis for understanding the case of a rotating active particle. We will demonstrate that the motion of a rotating active particle may be described by a decoupling between rotation events and the persistent motion during time intervals between rotations. Thus, we first need to understand the dynamics without rotation.

#### A. Exact theory using non-equilibrium correlators

To study the motion of a non-rotating active tracer, we note that in order for the particle to move in its active direction, it needs the five sites denoted  $a, b, c, d$ , and  $e$  in Fig. 2 to all be vacant. If we denote the occupancy of each site  $i$  by the indicator random variable  $\eta_i = 0, 1$ , then for a given configuration of the particles on the lattice, the ability to move in the active direction is given by

$$W_+ = (1 - \eta_a)(1 - \eta_b)(1 - \eta_c)(1 - \eta_d)(1 - \eta_e). \quad (1)$$

This variable may be equal to zero or one, with  $W_+ = 1$  meaning that the particle can move forward and  $W_+ = 0$  meaning that it cannot. To analyze the net flow in the active direction, we consider also the motion in the opposite direction, which in turn requires vacancy of all sites  $\tilde{a}, \tilde{b}, \tilde{c}, \tilde{d}$ , and  $\tilde{e}$ . The ability to move in the opposite direction is given by

$$W_- = (1 - \eta_{\tilde{a}})(1 - \eta_{\tilde{b}})(1 - \eta_{\tilde{c}})(1 - \eta_{\tilde{d}})(1 - \eta_{\tilde{e}}). \quad (2)$$

Now, the position  $r_{\parallel}(t)$  along the active direction of this non-rotating active tracer evolves according to the following stochastic

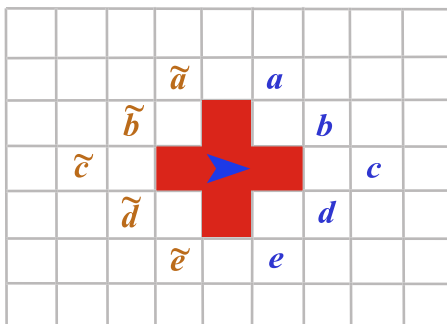


**FIG. 2.** Active tracer with its active direction denoted by a blue arrowhead. The sites, which must be vacant along the active direction, are denoted by  $a, b, c, d$ , and  $e$  and along the opposite direction by  $\tilde{a}, \tilde{b}, \tilde{c}, \tilde{d}$ , and  $\tilde{e}$ .

dynamics:

$$r_{\parallel}(t + dt) = \begin{cases} \text{value :} & \text{probability:} \\ r_{\parallel}(t) + 1 & p_+ \\ r_{\parallel}(t) - 1 & p_- \\ r_{\parallel}(t) & 1 - p_+ - p_-, \end{cases} \quad (3)$$

where  $p_+ = (R_T + R_A)W_+dt$  and  $p_- = R_T W_-dt$  are the probabilities to move in the forward and backward directions, respectively, during an infinitesimal time interval  $dt$ . Averaging over Eq. (3), we see that the average drift velocity of the active tracer is given by

$$v \equiv \frac{d\langle r_{\parallel}(t) \rangle}{dt} = (R_A + R_T)C_+ - R_T C_-, \quad (4)$$

where  $C_{\pm} = \langle W_{\pm} \rangle$  are the probabilities that the moves in the forward and backward directions are not blocked by other particles. Note that these probabilities depend on non-equilibrium correlations that develop in the close proximity of the active tracer due to its non-equilibrium motion, and thus, depend not only on density but also on activity.

We now expand the products in Eqs. (1) and (2). We note that due to the model's exclusion, some blocking sites may not be simultaneously occupied, for instance sites  $a$  and  $b$ . Therefore,  $\eta_a$  and  $\eta_b$  may not be both equal to one; thus,  $\langle \eta_a \eta_b \rangle = 0$ . By canceling all such terms that are identically zero, we may write

$$C_+ = \left( 1 - \langle \eta_a \rangle - \langle \eta_b \rangle - \langle \eta_c \rangle - \langle \eta_d \rangle - \langle \eta_e \rangle + \langle \eta_a \eta_c \rangle + \langle \eta_a \eta_d \rangle + \langle \eta_a \eta_e \rangle + \langle \eta_b \eta_e \rangle + \langle \eta_c \eta_e \rangle - \langle \eta_a \eta_c \eta_e \rangle \right). \quad (5)$$

Sites  $a$  and  $e$  are symmetric and also  $b$  and  $d$ , so this may be further simplified to the following form:

$$C_+ = \left( 1 - 2\langle \eta_a \rangle - 2\langle \eta_b \rangle - \langle \eta_c \rangle + 2\langle \eta_a \eta_c \rangle + 2\langle \eta_a \eta_d \rangle + \langle \eta_a \eta_e \rangle - \langle \eta_a \eta_c \eta_e \rangle \right), \quad (6)$$

and for the backward direction, we similarly obtain

$$C_- = \left( 1 - 2\langle \eta_{\tilde{a}} \rangle - 2\langle \eta_{\tilde{b}} \rangle - \langle \eta_{\tilde{c}} \rangle + 2\langle \eta_{\tilde{a}} \eta_{\tilde{c}} \rangle + 2\langle \eta_{\tilde{a}} \eta_{\tilde{d}} \rangle + \langle \eta_{\tilde{a}} \eta_{\tilde{e}} \rangle - \langle \eta_{\tilde{a}} \eta_{\tilde{c}} \eta_{\tilde{e}} \rangle \right). \quad (7)$$

We note that Eq. (4) is exact. However, it requires the high-order non-equilibrium density correlations which appear in Eqs. (6) and (7). Even without a theoretical framework for analytically calculating these correlations, we may obtain them from numerical simulations. Figure 3 shows the perfect agreement between the direct measurement of the drift velocity  $v$  in numerical simulations and the evaluation of Eq. (4) using the correlations of Eqs. (6) and (7) obtained in the same numerical simulations. Note that these are non-equilibrium simulations which include the active tracer in them.

Figure 3, and specifically its inset with normalized velocity vs normalized activity, shows how the drift velocity exhibits a crossover from a linear response at low  $R_A$  to saturation to an asymptotic value at high  $R_A$ . We may fit this by the following functional form:

$$\frac{1}{v} = \frac{1}{\mu R_A} + \frac{1}{v_{\infty} R_T}, \quad (8)$$

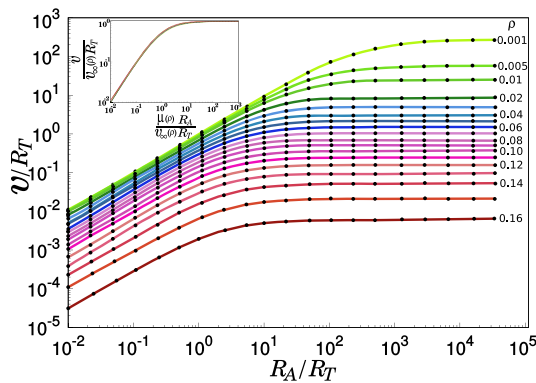


**FIG. 3.** The drift velocity of a non-rotating active tracer. Measuring the correlators of Eqs. (6) and (7) from numerical simulation and plugging them in Eq. (4), lines, perfectly agrees with direct measurement of the drift velocity in simulation, points. Numbers next to each line indicate density values. Inset: normalized velocity vs normalized activity perfectly collapse to a single curve. Colored lines correspond to different densities as in the main plot. Black line is Eq. (8).

where  $\mu$  is the mobility and  $v_\infty$  is the asymptotic velocity. Characterizing the entire dependence on  $R_A$  thus boils down to understanding these two limits. We will now see which parts of the behavior that we observe here can be obtained using only equilibrium properties of the passive system. Subsequently we will provide some theoretical justification for the functional form of Eq. (8).

### B. Tracer dynamics for low $R_A$

Before proceeding, we note that if we ignore correlations, we may obtain for the low-density limit a mean-field approximation. To this end, we set in Eqs. (6) and (7),  $\langle \eta_i \rangle = \rho$ ,  $\langle \eta_i \eta_j \rangle = \rho^2$ , and  $\langle \eta_i \eta_j \eta_k \rangle = \rho^3$ . Thus, we may write

$$C_+ = C_- = C_{MF} = 1 - 5\rho + 5\rho^2 - \rho^3, \quad (9)$$

which yields the following mean-field drift velocity,  $v_{MF} = R_A C_{MF}$ .

As seen in Fig. 3, at low  $R_A$ , by linear response, the drift velocity  $v$  is linearly proportional to  $R_A$ , and we may define the mobility as

$$\mu = \lim_{R_A \rightarrow 0} \frac{v}{R_A}. \quad (10)$$

We first note that the mean-field mobility is equal to  $\mu_{MF} = C_{MF}$ , which is given in Eq. (9) above.

Now, given Eq. (4), we expand  $C_\pm$  to linear order in  $R_A$ ,

$$C_\pm(\rho, R_A) = C_0(\rho) + C'_\pm(\rho)R_A, \quad (11)$$

where prime indicates derivative with respect to  $R_A$  at  $R_A = 0$ . Thus,

$$\mu = C_0 + R_T \delta C, \quad (12)$$

where  $\delta C \equiv C'_+ - C'_-$ . That is, the mobility depends not only on the equilibrium value  $C_0$  but also on the forward-backward asymmetry encoded in  $\delta C$ . Figure 4 first shows that the Stokes-Einstein relations hold, namely, the mobility exactly coincides with the self-diffusion coefficient,  $D_T$  measured from the long-time mean-squared

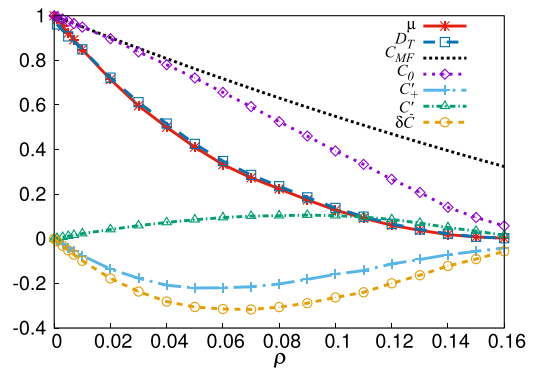


**FIG. 4.** Mobility and its different components vs density. Mobility  $\mu$  perfectly agrees with the diffusion coefficient  $D_T$ . Mean-field result  $C_{MF}$  agrees with  $C_0$  at low densities. However, even there, the additional terms in Eq. (12), namely,  $\delta C = C'_+ - C'_-$ , are significant.

displacement in a passive system,  $\langle \Delta r^2 \rangle = 4D_T t$ . Second, the figure shows that the mean-field mobility  $C_{MF}$  [Eq. (9)] describes well the low-densities behavior of the equilibrium correlator  $C_0$ . Finally, and most importantly, Fig. 4 shows how  $\delta C$  causes the actual mobility data to substantially deviate from  $C_0$ , which encodes only equilibrium properties. We can say that  $C'_+ < 0$  since due to the active motion, with increasing activity neighboring sites in the forward direction are more likely to be occupied. Similarly  $C'_- > 0$  because in the backward direction, with increasing activity sites are more likely to be vacant. However, at this point, we do not have even a low-density approximate theory for  $C'_+$  or  $C'_-$ .

To emphasize the importance of non-equilibrium information even at low activity and low density, we show in Fig. 5 the extremely low-density behavior of each of the lines from Fig. 4. As expected, all exhibit linear dependence on density, with  $C_0 \approx C_{MF} \approx 1 - 5\rho$ ,  $C'_+ \approx -8\rho$ , and  $C'_- \approx 2\rho$ . Thus,  $\delta C \approx -10\rho$ , and  $\mu \approx 1 - 15\rho$ . This numerically demonstrates the huge effect that non-equilibrium behavior has on the near-equilibrium behavior of the system. The equilibrium properties of the system are far from being able to describe the small deviations from equilibrium encoded in the mobility.

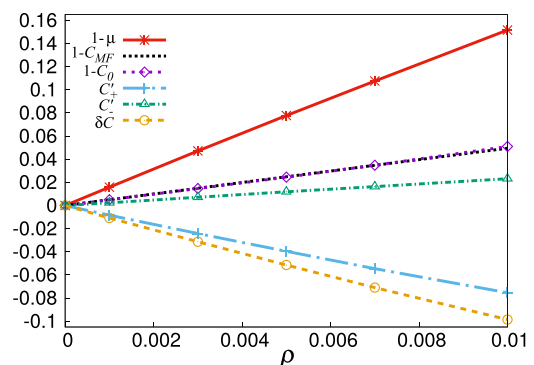


**FIG. 5.** Low-density behavior of the different components of the mobility. The non-equilibrium part  $\delta C$  has a larger contribution than the equilibrium part  $C_0$ .

### C. Tracer dynamics for high $R_A$

At large activity, the drift velocity  $v$  of the tracer reaches a density-dependent asymptotic value  $v_\infty$ , as seen in Fig. 3. For extremely large  $R_A$ , once the active tracer can move in its active direction, it will immediately move. Hence, it spends almost all of the time waiting for a thermal move to free it and so to enable the active motion to resume. Here we develop a theoretical description for this process that will be valid in the low-density limit. At large  $R_A$ , we assume that the tracer moves rapidly into a region which has not been perturbed by its motion. The motion of the tracer involves instantaneous active flights between obstructions, along with periods spent waiting for an obstruction to be removed by a thermal move. We will begin by studying the case of infinite  $R_A$  and then discuss how to include finite  $R_A$ .

We can describe this process as a continuous-time random-walk with steps of length  $\ell_i$ , along which the tracer moves in its active direction without meeting any passive particles that block its motion; see Fig. 6. At the end of each such flight, the tracer has to wait for a time  $\tau_i$  before it can begin its next flight. Assuming these two events are uncorrelated, the asymptotic drift velocity is given by the ratio between the average distance  $\langle \ell \rangle$  traveled in each step and the average waiting time  $\langle \tau \rangle$  at the end of each step. Note the similarity of this approach to that used in Ref. 33.

We first compute the average distance between obstructions  $\langle \ell \rangle$ , assuming the system around the active tracer to be in equilibrium. Therefore,  $\langle \ell \rangle$  depends only on the equilibrium density  $\rho$ . For low densities, at each new site the active tracer reaches, the probability that it will be able to continue to one more site is equal to the equilibrium value  $C_0(\rho)$ , discussed above. So the probability of encountering an obstruction is  $1 - C_0(\rho)$ . Treating obstructions as a Poisson process with density  $1 - C_0(\rho)$ , the distribution of gaps between them is given by  $p(\ell) = (1 - C_0) \exp[-(1 - C_0)\ell]$ . Thus, the average distance that the active tracer travels until reaching a passive

particle that blocks it is equal to

$$\langle \ell \rangle = \frac{1}{1 - C_0(\rho)}. \quad (13)$$

Next, we compute the average waiting time  $\langle \tau \rangle$  at the end of each active flight. Once the active tracer meets a passive particle, it waits for a duration  $\tau$  until it can continue its flight along its active direction. Therefore, the active tracer must wait until the passive particle moves out of its way or alternatively until the active particle itself moves laterally and the passive particle no longer blocks its motion along the active direction. For the active particle to be unblocked, the five sites  $a, b, c, d,$  and  $e$  in front of it should be vacant (see Fig. 2). In the low-density limit, we may consider only single-particle blocking mechanisms. We consider a blocking particle to be in each one of the five blocking sites,  $a, b, c, d,$  or  $e$ . Each of these cases can have different average waiting times; however, symmetry dictates  $\langle \tau_a \rangle = \langle \tau_e \rangle$  and  $\langle \tau_b \rangle = \langle \tau_d \rangle$ . Since these cases all involve single particle obstructions, each occurs with an equal probability that depends only on  $\rho$ . Therefore, we can write the average waiting time for unblocking as

$$\langle \tau \rangle = \frac{2}{5} \langle \tau_a \rangle + \frac{2}{5} \langle \tau_b \rangle + \frac{1}{5} \langle \tau_c \rangle. \quad (14)$$

When the active tracer meets a blocking particle at site  $a$ , it has to wait until either the active particle thermally moves downwards, or the blocking particle thermally moves upwards; see Fig. 6(a). Each one of these processes occurs at rate  $R_T$ ; thus, the average time until one of them occurs is equal to  $\langle \tau_a \rangle = \frac{1}{2R_T}$ . Note that the particle at  $a$  can also move forward (to the right in the figure). However, then the active tracer would immediately move forward and would still be blocked by this passive particle. We do not consider that as an unblocking event because it merely increases  $\ell$  by one. Since  $\ell$  is much larger than one, this move has a negligible effect on  $\langle \ell \rangle$ .

If the blocking particle is at site  $b$ , due to the same argument, we ignore its motion in the forward direction and only consider the lateral motion. For the active tracer to overcome the blocking by this particle, these two particles should make two consecutive thermal moves in the lateral direction—the thermal particle upwards and the active particle downwards; see Fig. 6(b). Each single move occurs at rate  $R_T$ ; thus, the average time until either one moves one step laterally is  $\frac{1}{2R_T}$ , and the total time until two such lateral moves occur is equal to  $\langle \tau_b \rangle = \frac{1}{R_T}$ .

For site  $c$ , the first move can be one of four, see Fig. 6(c), and thus, takes an average time  $\frac{1}{4R_T}$ . It should then be followed by two more moves, that each has two options, similarly to the sequence of unblocking after meeting a particle at site  $b$ . This eventually leads to  $\langle \tau_c \rangle = \frac{1}{4R_T} + \frac{2}{2R_T} = \frac{5}{4R_T}$ . Plugging  $\langle \tau_a \rangle$ ,  $\langle \tau_b \rangle$ , and  $\langle \tau_c \rangle$  in Eqs. (13) and (14) leads to the following approximation for the asymptotic drift velocity:

$$v_\infty = \frac{\langle \ell \rangle}{\langle \tau \rangle} = \frac{20R_T}{17(1 - C_0)}. \quad (15)$$

Figure 7 shows the agreement of this expression with the numerical results. We emphasize that in the low-activity limit, we could not obtain a result for the drift velocity purely in terms of

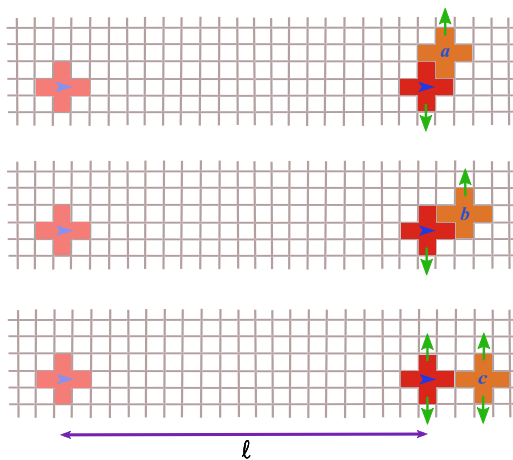


**FIG. 6.** Possible encounters of an active tracer (red) with a passive particle (orange) in the low-density, high-activity limit. The faded red crosses indicate the preceding position at which the active tracer encountered a passive particle. The green arrows indicate the moves of the active tracer or of the passive particle that would lead to unblocking and will enable the active tracer to continue moving along its active direction.

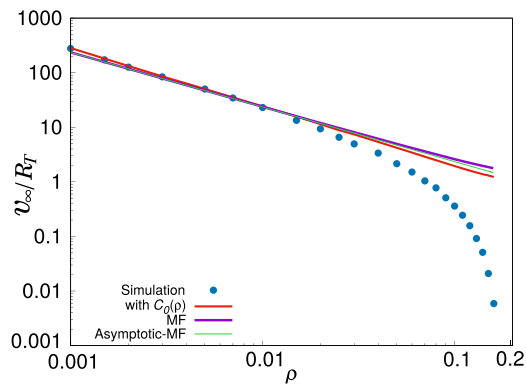


**FIG. 7.** Asymptotic, infinite  $R_A$  drift velocity of non-rotating active tracer. Theory (lines) describes the low-density behavior of the simulation results (blue dots). In this low-density range, using the numerically obtained correlation  $C_0(\rho)$ , Eq. (15) does not differ that much compared to using the mean-field result, Eq. (16) or its asymptotic behavior, Eq. (17).

properties of the equilibrium system. However, in the high-activity limit studied here, we can further simplify Eq. (15) by substituting the mean-field expression  $C_{MF}$  from Eq. (9) to get

$$v_{\infty}^{MF} = \frac{20R_T}{17(5\rho - 5\rho^2 + \rho^3)}. \quad (16)$$

In the low-density limit, this may be further approximated to the following asymptotic form:

$$v_{\infty}^{AMF} = \frac{4R_T}{17\rho}. \quad (17)$$

Since the theory developed here, and leading to Eq. (15), was valid for low densities in the first place, the agreement with numerical simulations shown in Fig. 7 is only at low densities, where the differences between the different expressions (15)–(17) are very small.

The theory developed here for the infinite  $R_A$  limit can also be extended to finite  $R_A$ . In that case, a finite amount of time is required for the motion of the tracer during active flights between obstructions. In the zero-density limit, between such stops, the active tracer moves freely at a speed  $R_A$ ; thus, the average time taken for the tracer to travel the average flight length is equal to  $\frac{\langle \ell \rangle}{R_A}$ . However, we know from the low- $R_A$  analysis in Sec. III B that with increasing density, the flight velocity is reduced to  $\mu(\rho)R_A$ . Thus, Eq. (15) is generalized to give the following expression for the drift velocity:

$$v = \frac{\langle \ell \rangle}{\frac{\langle \ell \rangle}{\mu(\rho)R_A} + \langle \tau \rangle}, \quad (18)$$

which has the functional dependence on  $R_A$  that we observed numerically in Fig. 3. See also Eq. (8).

## IV. ROTATION WITHOUT LOCKING

### A. Zero-density limit

We will begin the derivation with the zero-density limit of a single isolated tracer and will later introduce the effect of density. In

this limit, a passive tracer moves at rate  $R_T$  to each one of its four neighboring sites. Thus, the stochastic evolution of its position may be written as

$$x(t + dt) = \begin{cases} \text{value :} & \text{probability:} \\ x(t) + 1 & R_T dt \\ x(t) - 1 & R_T dt \\ x(t) & 1 - 2R_T dt. \end{cases} \quad (19)$$

Squaring and averaging over the stochasticity leads to

$$\langle x^2(t + dt) \rangle = \langle x^2(t) \rangle + 2R_T dt, \quad (20)$$

thus,  $\langle x^2(t) \rangle = 2R_T t$ , and by symmetry,  $\langle r^2(t) \rangle = \langle x^2(t) + y^2(t) \rangle = 4R_T t$ . Thus, the diffusion coefficient of this passive tracer equals  $D_T \equiv \frac{\langle r^2(t) \rangle}{4t} = R_T$ .

For an active tracer that rotates at rate  $R_R$  without locking, we divide time into intervals  $\Delta t_i$  between consecutive rotations. During each time interval, we identify the direction parallel to the current active direction and the direction perpendicular to that direction. In the perpendicular direction, the active tracer performs a random walk solely due to passive moves; thus,  $\langle \Delta r_{\perp}^2(\Delta t) \rangle = 2R_T \Delta t$ . For the parallel direction, in the present zero-density limit, we employ Eq. (3) with  $p_+ = R_T + R_A$  and  $p_- = R_T$ . By averaging, we get a drift  $\langle \Delta r_{\parallel}(t) \rangle = R_A t$ . By squaring Eq. (3) and averaging, we obtain

$$\langle r_{\parallel}^2(t + dt) \rangle = \langle r_{\parallel}^2(t) \rangle + (2R_T + R_A)dt + 2R_A \langle r_{\parallel}(t) \rangle dt. \quad (21)$$

By dividing by  $dt$ , substituting the drift expression obtained above, and integrating over a time interval  $\Delta t$  between rotations, we get

$$\langle \Delta r_{\parallel}^2(\Delta t) \rangle = (2R_T + R_A)\Delta t + R_A^2 \Delta t^2. \quad (22)$$

We now average over multiple such intervals. Each interval has different parallel and perpendicular directions and different durations. Rotation to each one of the two directions occurs at rate  $R_R$ ; thus, the time intervals between rotations have a Poisson distribution  $P(\Delta t) = 2R_R \exp(-2R_R \Delta t)$ . We may, therefore, write  $\langle \Delta t \rangle = \frac{1}{2R_R}$  and  $\langle \Delta t^2 \rangle = \frac{1}{2R_R^2}$ ; thus,  $\langle \Delta t^2 \rangle = \frac{\langle \Delta t \rangle^2}{R_R}$ . The different time intervals have their parallel and perpendicular directions randomly in the positive and negative  $x$  and  $y$  directions; thus, cross terms vanish and we may write

$$\begin{aligned} \langle \Delta r^2 \rangle &= \langle \Delta r_{\parallel}^2 \rangle + \langle \Delta r_{\perp}^2 \rangle = (4R_T + R_A)\langle \Delta t \rangle + R_A^2 \langle \Delta t^2 \rangle \\ &= \left( 4R_T + R_A + \frac{R_A^2}{R_R} \right) \langle \Delta t \rangle, \end{aligned} \quad (23)$$

and we obtain the following expression for the diffusion coefficient:

$$D_0 = \frac{\langle \Delta r^2 \rangle}{4\langle \Delta t \rangle} = R_T + \frac{R_A}{4} + \frac{R_A^2}{4R_R}, \quad (24)$$

where subscript 0 indicates the zero-density limit assumed above. We will discuss the different terms after extending this to finite densities.

### B. Including finite-density effects

For finite density, the attempt rates for motion are given by  $R_T$  and  $R_A$ , but due to the occupation of neighboring sites, not all

attempts succeed. The long-time behavior of a passive particle is diffusive with the passive diffusion coefficient  $D_T(\rho)$  discussed above (see Fig. 4). Thus, we assume that our active tracer has probabilities  $D_T(\rho)$  per unit time to perform thermal moves to each one of its four nearest neighbors. Similarly, during an interval between rotations, the active moves yield the drift velocity  $v(\rho, R_A)$  discussed above (see Fig. 3), and we hence assume that the tracer has an additional probability  $v(\rho, R_A)$  per unit time to move in its active direction. Under this assumption that ignores temporal correlations in the success probabilities of attempted moves, we may replace  $R_T$  in the zero-density derivation [Eq. (24) above] by  $D_T(\rho)$ , and  $R_A$  by  $v(\rho, R_A)$ , leading to

$$D = D_T(\rho) + \frac{v(\rho, R_A)}{4} + \frac{v^2(\rho, R_A)}{4R_R}. \quad (25)$$

We assumed that the passive and active motions are uncorrelated random processes; thus, the total diffusion coefficient we obtained is equal to the diffusion coefficient in the passive case, plus the diffusion coefficient resulting from the active process. The last term is similar to what we would get for an active Brownian particle.<sup>14</sup> However, the second term, which is linear in the drift velocity is a result of the discrete nature of the motion on the lattice.<sup>41</sup> One way to understand this term is to consider the fast rotation limit,  $R_R \gg R_A$ . In that limit, each time an active move is attempted, the active direction has been completely randomized, and the added rate  $R_A$  may be thought to be uniformly distributed between the rates of moving in all four directions; thus, the tracer undergoes passive motion with an effective thermal rate  $R_T + \frac{R_A}{4}$ .

Note that in the derivation of Eq. (25), we assumed that the active tracer moves at velocity  $v(\rho, R_A)$  between rotations. In practice, this velocity is obtained only after some time, and this derivation should be valid only for low enough rotation rate. To test this, we show in Fig. 8  $D - D_T$  vs  $v$  for multiple  $\rho$  and  $R_A$  values, where each color corresponds to a different value of  $R_R$ , as indicated in the legend. The figure shows nice data collapse and agreement with Eq. (25) even at high  $R_R$ .

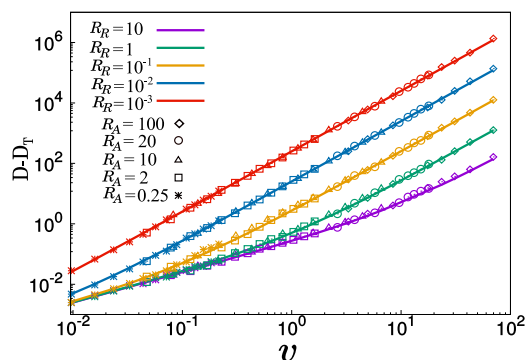


**FIG. 8.** Active part of the diffusion coefficient of an active tracer that rotates without rotational locking, plotted vs the drift velocity, as obtained from simulations without rotation. For each  $R_A$  and  $R_R$  values, we present results for densities ranging between  $\rho = 0.01$  and  $\rho = 0.13$ . The solid lines represent  $\frac{v}{4} + \frac{v^2}{4R_R}$ , as predicted by Eq. (25).

## V. ROTATIONAL LOCKING

When rotational locking is included, with increasing density not all rotation attempts succeed; thus, the rotational diffusion coefficient, or the actual rotation rate  $Q_R$ , is slower than the rotation attempt rate  $R_R$ , and the diffusion coefficient is smaller, in agreement with Eq. (25). We now show how this argument may yield also a quantitative prediction. Namely, we measure the actual rotation rate  $Q_R$  in simulations with rotational locking and assume that we may generalize Eq. (25) to include  $Q_R$ , instead of  $R_R$

$$D = D_T(\rho) + \frac{v(\rho, R_A)}{4} + \frac{v^2(\rho, R_A)}{4Q_R}, \quad (26)$$

where with locking  $Q_R < R_R$ , while without locking  $Q_R = R_R$ . Figure 9 shows that when plotted vs  $Q_R$ , results with and without locking perfectly agree. We could obtain numerical results only for densities  $\rho \leq 0.13$  since at higher densities, the dynamics are extremely slow, both due to the low drift velocity and due to rotational locking, which dramatically slows down the eventual rotation rate. Nonetheless, we expect that even as the density increases, Eq. (26) should describe the long-time diffusive behavior.

To complete the description of the rotational-locking case, we now study the dependence of the rotation acceptance probability  $P_R = Q_R/R_R$  on  $\rho$ ,  $R_A$ , and  $R_R$ . In order for a rotation attempt to succeed, all fourth-order neighbors of the active tracer should be vacant. Using the notations of Fig. 2, we can formally write this as

$$P_R = \langle (1 - \eta_a)(1 - \eta_b)(1 - \eta_d)(1 - \eta_e) \times (1 - \eta_{\bar{a}})(1 - \eta_{\bar{b}})(1 - \eta_{\bar{d}})(1 - \eta_{\bar{e}}) \rangle. \quad (27)$$

We now expand this product, and similarly to the process leading to Eq. (5), we note that not all fourth-order neighbors may be occupied simultaneously. Assuming mean-field occupations, this leads to the following approximation for the rotation probability:

$$P_R^{MF} = 1 - 8\rho + 20\rho^2 - 16\rho^3 + 2\rho^4. \quad (28)$$

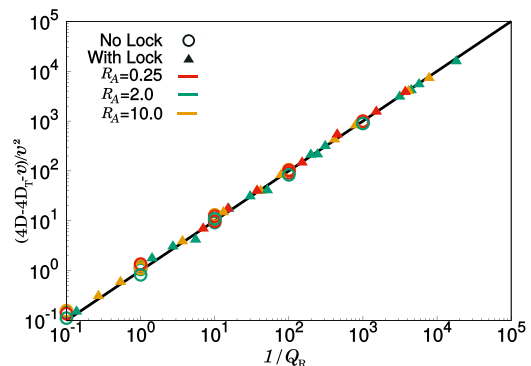


**FIG. 9.** Agreement with Eq. (26) of data from simulations with (solid symbols) and without (open symbols) rotational locking. Data collapses to the identity line, while all three parameters,  $\rho$ ,  $R_T$ , and  $R_R$  were varied for an arbitrary choice of  $R_T = 1$ .

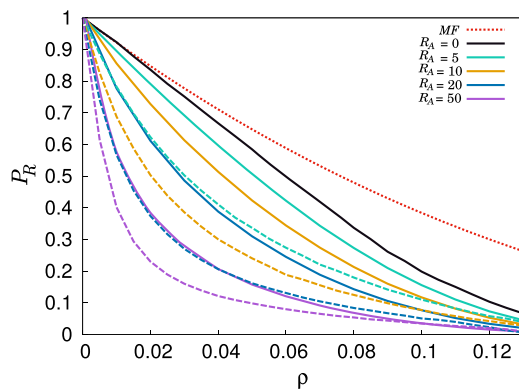


**FIG. 10.** Rotation acceptance rate  $P_R = Q_R/R_R$  vs density  $\rho$  for the passive case ( $R_A = 0$ ) agrees with mean field theory (28) at low density.  $P_R$  decreases with increasing activity ( $R_A > 0$ ). Continuous lines correspond to the high  $R_R$  limit ( $R_R = 100$ ), and dashed lines correspond to the low  $R_R$  limit ( $R_R = 0.01$ ).

Figure 10 shows that in the passive case ( $R_A = 0$ ), at low densities the numerically obtained rotation probability  $P_R$  agrees with this mean-field approximation.

Following the arguments of Sec. III C above, with increasing activity, the active tracer spends more of its time in denser regions, waiting for passive particles to move out of its way. During that time, its rotation probability is decreased. In Fig. 10, we indeed see how  $P_R$  decreases with increasing activity. In Fig. 11, we show the  $R_R$  dependence of  $P_R$ . Specifically we see independence on  $R_R$  at both low- and high- $R_R$  limits. This may be understood as follows: At low  $R_R$ , there is a very long time between rotation attempts, and the tracer's environment gets randomized so that consecutive rotation events are independent; thus, decreasing  $R_R$  even more does not change the success rate. Similarly, for large  $R_R$  rotation attempts occur so rapidly that the particle hardly moves between them; thus, increasing  $R_R$  further does not change  $P_R$ . Note that at intermediate  $R_R$ , we may observe a modest dip in  $P_R$  (see, for example,  $\rho = 0.01$ ,  $R_A = 10$  in Fig. 11). It would be interesting to get a better, quantitative understanding of the dependence of  $P_R$  on  $\rho$ ,  $R_A$ , and  $R_R$ . However, we defer that to future publications.

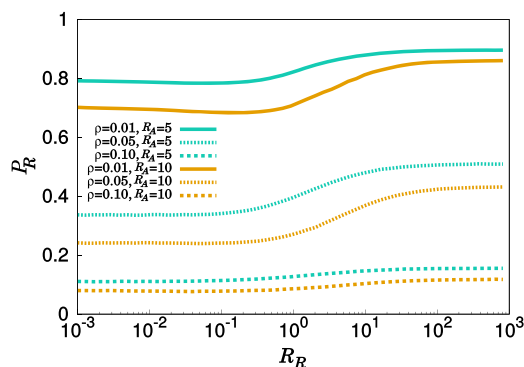


**FIG. 11.** Rotation acceptance rate  $P_R = Q_R/R_R$  increases with increasing  $R_R$  but saturates both at low  $R_R$  and at high  $R_R$ .

## VI. DISCUSSION

We consider the lattice-gas model with exclusion up to third-order neighbors on the square lattice. Due to this exclusion, the particles in this model are equivalent to hard, cross-shaped pentamers. This model has an equilibrium first-order phase transition with coexistence between fluid at density  $\rho_m \approx 0.16$  and crystal at density  $\rho_x \approx 0.19$  and exhibits a glass transition at  $\rho_g \approx 0.17$ . We added activity to this model by assigning an active direction of self-propulsion to the particles. With time, this direction may undergo rotational diffusion. The cross shape of the particles enabled us to naturally introduce a locking mechanism that prevents rotation due to the presence of neighboring particles. Our ultimate goal is to use this model to study the interplay between the activity and jamming. This will advance the understanding of the cooperative phenomena that govern closely-packed active matter systems.

In this paper, we focused on the case of a single active tracer in a bath of thermal particles. At long times, this tracer undergoes diffusive motion, and for the case without rotational locking, we could write its self-diffusion coefficient in terms of (i) the diffusion coefficient  $D_T(\rho)$  of a passive particle, (ii) the drift velocity  $v(R_A, \rho)$  of a non-rotating active tracer, and (iii) the rotation rate  $R_R$ . Remarkably, when rotational locking is introduced, it merely reduces the rate of successful rotations, and when the rate  $Q_R$  at which rotations occur is used, instead of the rate  $R_R$  of rotation attempts, our theoretical prediction perfectly matches the results of our numerical simulations.

Interestingly, we showed that the properties of the passive system are not enough to fully describe the drift velocity of a non-rotating active tracer, not even in the low-activity and low-density limit. Here, we expect the system to be close to equilibrium, yet we could not describe the dynamics of the tracer using only knowledge of the equilibrium properties of the system. Thus, even in the low-density limit where equilibrium correlations vanish, the mean-field approximation does not work. It is interesting to note that a similar phenomenon has recently been studied in the context of bulk diffusion in lattice-gas models.<sup>42–45</sup> Nonetheless, we developed a theory in terms of equilibrium correlators, which applies for low density and strong activity.

There are several interesting directions to explore. We can add a small but finite density of active tracers to the thermal lattice gas, in which case interactions between the active particles, mediated through the bath, can show interesting effects. Our study can also serve as the basis for the investigation of this model when all the particles are active. For such an all-active system, we also expect to be able to understand the long-time diffusive behavior of a rotating particle in terms of its drift velocity during intervals between rotations. And we expect to be able to describe the effect of rotational locking as reducing the rotation rate.

Finally, we note that in this paper we focused on a lattice gas model, for which we can reach a very detailed theoretical understanding of the physical phenomena. We expect much of the insight we gained in this model to also be applicable to more general continuous systems. Specifically, it would be interesting to consider in other systems the separation between active drift velocity and rotational diffusion, as well as the effects of rotational locking with increasing density.

## ACKNOWLEDGMENTS

We thank Gregory Bolshak, Abhishek Dhar, Arghya Das, Arnab Pal, Shlomi Reuveni, and Eial Teomy for helpful discussions. This work was partially supported by the Israel Science Foundation, Grant No. 968/16, and by a grant from the United States-Israel Binational Science Foundation. C.M. and B.C. have been supported by the Brandeis MRSEC through NSF-DMR 1420382. K.R. and B.C. have been supported by a grant from the W. M. Keck Foundation.

## REFERENCES

- <sup>1</sup>B. R. Parry, I. V. Surovtsev, M. T. Cabeen, C. S. O'Hern, E. R. Dufresne, and C. Jacobs-Wagner, *Cell* **156**, 183 (2014).
- <sup>2</sup>A. Chaudhuri, B. Bhattacharya, K. Gowrishankar, S. Mayor, and M. Rao, *Proc. Natl. Acad. Sci. U. S. A.* **108**, 14825 (2011).
- <sup>3</sup>T. E. Angelini, E. Hannezo, X. Trepate, M. Marquez, J. J. Fredberg, and D. A. Weitz, *Proc. Natl. Acad. Sci. U. S. A.* **108**, 4714 (2010).
- <sup>4</sup>D. Bi, X. Yang, M. C. Marchetti, and M. L. Manning, *Phys. Rev. X* **6**, 021011 (2015).
- <sup>5</sup>X. Chen, X. Dong, A. Be'er, H. L. Swinney, and H. P. Zhang, *Phys. Rev. Lett.* **108**, 148101 (2012).
- <sup>6</sup>J. L. Silverberg, M. Bierbaum, J. P. Sethna, and I. Cohen, *Phys. Rev. Lett.* **110**, 228701 (2013).
- <sup>7</sup>Y. Fily and M. C. Marchetti, *Phys. Rev. Lett.* **108**, 235702 (2012).
- <sup>8</sup>G. S. Redner, M. F. Hagan, and A. Baskaran, *Phys. Rev. Lett.* **110**, 055701 (2013).
- <sup>9</sup>M. E. Cates and J. Tailleur, *Annu. Rev. Condens. Matter Phys.* **6**, 219 (2015).
- <sup>10</sup>J. Bialke, T. Speck, and H. Lowen, *Phys. Rev. Lett.* **108**, 168301 (2012).
- <sup>11</sup>Q. Liao and N. Xu, *Soft Matter* **14**, 853 (2018).
- <sup>12</sup>L. Berthier, *Phys. Rev. Lett.* **112**, 220602 (2014).
- <sup>13</sup>R. Mandal, P. J. Bhuyan, M. Rao, and C. Dasgupta, *Soft Matter* **12**, 6268 (2016).
- <sup>14</sup>Y. Fily, S. Henkes, and M. C. Marchetti, *Soft Matter* **10**, 2132 (2014).
- <sup>15</sup>D. Levis and L. Berthier, *Phys. Rev. E* **89**, 062301 (2014).
- <sup>16</sup>G. S. Redner, M. F. Hagan, and A. Baskaran, *Phys. Rev. E* **88**, 012305 (2013).
- <sup>17</sup>G. Biroli and M. Mézard, *Phys. Rev. Lett.* **88**, 025501 (2001).
- <sup>18</sup>Z. Rotman and E. Eisenberg, *Phys. Rev. E* **80**, 060104 (2009).
- <sup>19</sup>M. Kourbane-Houssene, C. Erignoux, T. Bodineau, and J. Tailleur, *Phys. Rev. Lett.* **120**, 268003 (2018).
- <sup>20</sup>A. Bellemans and J. Orban, *Phys. Rev. Lett.* **17**, 908 (1966).
- <sup>21</sup>R. J. Baxter, *J. Phys. A: Math. Gen.* **13**, L61 (1980).
- <sup>22</sup>J. Orban and D. Van Belle, *J. Phys. A: Math. Gen.* **15**, L501 (1982).
- <sup>23</sup>M. Barma and D. Dhar, *Phys. Rev. Lett.* **73**, 2135 (1994).
- <sup>24</sup>E. Eisenberg and A. Baram, *J. Phys. A: Math. Gen.* **33**, 1729 (2000).
- <sup>25</sup>E. Eisenberg and A. Baram, *Europhys. Lett.* **71**, 900 (2005).
- <sup>26</sup>H. C. M. Fernandez, J. J. Arenzon, and Y. Levin, *J. Chem. Phys.* **126**, 114508 (2007).
- <sup>27</sup>B. C. Barnes, D. W. Siderius, and L. D. Gelb, *Langmuir* **25**, 6702 (2009).
- <sup>28</sup>Z. Rotman and E. Eisenberg, *Phys. Rev. Lett.* **105**, 225503 (2010).
- <sup>29</sup>R. Dickman, *J. Chem. Phys.* **136**, 174105 (2012).
- <sup>30</sup>K. Ramola and D. Dhar, *Phys. Rev. E* **86**, 031135 (2012).
- <sup>31</sup>T. Nath and R. Rajesh, *Phys. Rev. E* **90**, 012120 (2014).
- <sup>32</sup>O. Bénichou, P. Illien, G. Oshanin, and R. Voituriez, *Phys. Rev. E* **87**, 032164 (2013).
- <sup>33</sup>O. Bénichou, P. Illien, G. Oshanin, A. Sarracino, and R. Voituriez, *Phys. Rev. Lett.* **113**, 268002 (2014).
- <sup>34</sup>O. Bénichou, P. Illien, G. Oshanin, A. Sarracino, and R. Voituriez, *J. Phys.: Condens. Matter* **30**, 443001 (2018).
- <sup>35</sup>P. Illien, O. Bénichou, C. Mejía-Monasterio, G. Oshanin, and R. Voituriez, *Phys. Rev. Lett.* **111**, 038102 (2013).
- <sup>36</sup>T. Bertrand, Y. Zhao, O. Bénichou, J. Tailleur, and R. Voituriez, *Phys. Rev. Lett.* **120**, 198103 (2018).
- <sup>37</sup>T. Bertrand, P. Illien, O. Bénichou, and R. Voituriez, *New J. Phys.* **20**, 113045 (2018).
- <sup>38</sup>T. Chou, K. Mallick, and R. Zia, *Rep. Prog. Phys.* **74**, 116601 (2011).
- <sup>39</sup>T. M. Squires and T. G. Mason, *Annu. Rev. Fluid Mech.* **42**, 413 (2009).
- <sup>40</sup>S. Whitelam, K. Klymko, and D. Mandal, *J. Chem. Phys.* **148**, 154902 (2018).
- <sup>41</sup>O. Bénichou, K. Lindenberg, and G. Oshanin, *Physica A* **392**, 3909 (2013).
- <sup>42</sup>C. Arita, P. L. Krapivsky, and K. Mallick, *Phys. Rev. E* **90**, 052108 (2014).
- <sup>43</sup>E. Teomy and Y. Shokef, *Phys. Rev. E* **95**, 022124 (2017).
- <sup>44</sup>C. Arita, P. L. Krapivsky, and K. Mallick, *Phys. Rev. E* **95**, 032121 (2017).
- <sup>45</sup>E. Teomy, private communication (2018).
- <sup>46</sup>P. Digregorio, D. Levis, A. Suma, L. F. Cugliandolo, G. Gonnella, and I. Pagonabarraga, *Phys. Rev. Lett.* **121**, 098003 (2018).